

Huge quadratic magneto-optical Kerr effect and magnetization reversal in the Co_2FeSi Heusler compound

J. Hamrle, S. Blomeier, O. Gaier, B. Hillebrands

Fachbereich Physik and Forschungsschwerpunkt MINAS, Technische Universität Kaiserslautern, Erwin-Schrödinger-Straße 56, D-67663 Kaiserslautern, Germany

H. Schneider, G. Jakob

Institut für Physik, Johannes Gutenberg-Universität Mainz, Staudinger Weg 7, D-55128 Mainz, Germany

K. Postava

Department of Physics, Technical University of Ostrava, 17. listopadu 15, 708 33, Ostrava-Poruba, Czech Republic

C. Felser

Institute of Inorganic and Analytical Chemistry, Johannes Gutenberg-Universität Mainz, Staudingerweg 9, D-55128 Mainz, Germany

Abstract.

$\text{Co}_2\text{FeSi}(100)$ films with L_{21} structure deposited onto $\text{MgO}(100)$ were studied exploiting both longitudinal (LMOKE) and quadratic (QMOKE) magneto-optical Kerr effect. The films exhibit a huge QMOKE signal with a maximum contribution of up to 30 mdeg, which is the largest QMOKE signal in reflection that has been measured thus far. This large value is a fingerprint of an exceptionally large spin-orbit coupling of second or higher order. The $\text{Co}_2\text{FeSi}(100)$ films exhibit a rather large coercivity of 350 and 70 Oe for film thicknesses of 22 and 98 nm, respectively. Despite the fact that the films are epitaxial, they do not provide an angular dependence of the anisotropy and the remanence in excess of 1% and 2%, respectively.

1. Introduction

Since its discovery by John Kerr in 1877 [1] the magneto-optical Kerr effect (MOKE) has evolved into a very powerful investigational tool for magnetic materials. In most cases only first order contributions of MOKE are detected, i.e., only the contributions linearly proportional to the sample magnetization. In such a case (neglecting exchange bias systems), the measured MOKE loops are symmetric. The first order MOKE is divided into polar MOKE (PMOKE), which is proportional to the out-of-plane magnetization component, longitudinal MOKE (LMOKE), and transverse MOKE (TMOKE), with the two latter effects being proportional to the in-plane magnetization components parallel and perpendicular to the plane of light incidence, respectively. [2]

However, for some materials, for example Fe/MgO, [3], Fe/Ag, [4] and Py/Ta, [5] or even in diluted magnetic semiconductors as $\text{Ga}_{1-x}\text{Mn}_x\text{As}$, [6] asymmetric MOKE loops were observed. Osgood *et al.* [7] and Postava *et al.* [3] first attributed the asymmetric nature of such loops to a superimposed quadratic MOKE (QMOKE) contribution, exhibiting an even dependence on the applied magnetic field. Osgood *et al.* originally stated that the QMOKE signal is related only to the magnetization term $M_L M_T$, [7] and therefore concluded that QMOKE loops may only appear for systems where the magnetization reversal occurs by a coherent magnetization rotation, where M_L and M_T are the longitudinal and transverse magnetization components with respect to the plane of light incidence, respectively. However, it has been shown later that the QMOKE signal is proportional to two mixed terms, $M_L M_T$ and $M_L^2 - M_T^2$. [8] Hence, QMOKE contributions to magnetization curves may appear also in systems where magnetization reversal takes place by nucleation and growth of magnetic domains, as it is the case for the hysteresis loops presented in this article.

A non-zero Kerr effect requires the presence of both spin-orbit (SO) coupling and exchange interactions. [9, 10] The first order MOKE (both PMOKE and LMOKE) originates from a component of \mathbf{M} parallel to \mathbf{k} , where \mathbf{k} is a wavevector of light *inside* the ferromagnetic materials. In this configuration, the first order contribution to SO coupling, $E_{\text{SO}} = \xi \mathbf{L} \cdot \mathbf{S}$, is dominant. [7] On the other hand, the QMOKE originates from a component of \mathbf{M} perpendicular to the plane of incidence. In this situation, the first order of SO coupling is zero, $\xi \mathbf{L} \cdot \mathbf{S} = 0$. Therefore, only SO coupling of second or higher order can give rise to QMOKE. As such higher order contributions of SO coupling are usually much smaller than those of first order, the QMOKE is usually much smaller than the first-order MOKE.

In the present work we investigate the magneto-optical properties of the half-metallic $\text{Co}_2\text{FeSi}(100)$ Heusler compound, which recently attracted lots of attention as a possible candidate for spintronic applications. [11, 12, 13, 14, 15, 16, 17, 18] This compound exhibits the highest magnetic moment ($5.97 \mu_B$) per formula unit (at 5 K, corresponding to an average value of $1.49 \mu_B$ per atom) and the highest Curie temperature (1100 K) among all half-metallic ferromagnets investigated so far.[11] The magnetic moments per atom derived from a sum rule analysis are $2.6 \mu_B$ for Fe and

$1.2 \mu_B$ for Co at 300 K and 400 Oe.[16] For those reason, a thorough characterization of the magnetic properties of this material is of great interest from a technological point of view. However, the magneto-optical properties of Co₂FeSi have not yet been studied in detail. Here we perform such an investigation, and in this context we demonstrate that the material under investigation exhibits the highest QMOKE that has ever been measured so far in a magnetic thin film system.

2. Theory of the longitudinal and quadratic MOKE

In order to facilitate the understanding of this work, we now briefly summarize the physical origin and theoretical description of both first order MOKE and QMOKE.

A cartesian coordinate system which will be used throughout this article is sketched in Fig. 1. The z -axis of this system corresponds to the sample out-of-plane axis, while the in-plane y - and x -axes are parallel and perpendicular to the plane of light incidence, respectively. The sample orientation is described by an angle α , which is the angle between the y -axis and the in-plane [100] direction of the crystal lattice. In the following, the relative sample magnetization components along the y and the x axis are called longitudinal M_L and transversal M_T magnetization, respectively. Note that M_L and M_T are defined with respect to the plane of light incidence and not with respect to the orientation of the sample or with respect to the applied magnetic field.

The optical and magneto-optical properties of a magnetized crystal are described by the permittivity tensor ε_{ij} , which can be developed into a series in the components of the sample magnetization \mathbf{M} :

$$\varepsilon_{ij} = \varepsilon_{ij}^{(0)} + K_{ijk}M_k + G_{ijkl}M_kM_l + \dots, \quad (1)$$

where the M_i are the components of \mathbf{M} . In Eq. (1) the Einstein summation convention over the x , y , and z coordinates is used. The $\varepsilon_{ij}^{(0)}$, K_{ijk} and G_{ijkl} are constants, forming the dielectric tensor and the linear and quadratic magneto-optical tensors, respectively. [19] The number of independent components of these tensors can be reduced using the Onsager relation

$$\varepsilon_{ij}(\mathbf{M}) = \varepsilon_{ji}(-\mathbf{M}) \quad (2)$$

which can also be written in form of general symmetry arguments [19, 20]

$$\begin{aligned} \varepsilon_{ij}^{(0)} &= \varepsilon_{ji}^{(0)} \\ K_{ijk} &= -K_{jik}, \quad K_{iik} = 0, \quad i \neq j \neq k \\ G_{ijkl} &= G_{jikl} = G_{jilk} = G_{ijlk}. \end{aligned} \quad (3)$$

For cubic crystals (as in the case of Co₂FeSi(100) studied here), the number of independent tensor elements can be reduced further, resulting in only one free (complex) parameter in the constant term $\varepsilon_{ij}^{(0)}$, another one in the linear term K_{ijk} and three additional parameters in the quadratic term G_{ijkl} (note that the general symmetry

relations determined by Eq. (3) are still valid) [20]

$$\begin{aligned}
 \varepsilon_{ij}^{(0)} &= \varepsilon_d \delta_{ij} \\
 K_{ijk} &= K \\
 G_{iiii} &= G_{11} \\
 G_{iijj} &= G_{12}, \quad i \neq j \\
 G_{1212} &= G_{1313} = G_{2323} = G_{44} \quad ,
 \end{aligned} \tag{4}$$

with δ_{ij} being the Kronecker delta-function. Therefore, the off-diagonal elements of ε_{ij} can be written as (here we limit ourselves to in-plane magnetization only):

$$\begin{aligned}
 \varepsilon_{xy} &= \varepsilon_{yx} = 2G_{44}M_LM_T \\
 \varepsilon_{xz} &= -\varepsilon_{zx} = KM_L \\
 \varepsilon_{yz} &= -\varepsilon_{zy} = -KM_T \quad .
 \end{aligned} \tag{5}$$

On the other hand, at a sample orientation of $\alpha \neq 0$ the off-diagonal permittivity tensor elements can be written as

$$\begin{aligned}
 \varepsilon_{xy} &= \varepsilon_{yx} = \left[2G_{44} + \frac{\Delta G}{2}(1 - \cos 4\alpha) \right] M_LM_T - \frac{\Delta G}{4} \sin 4\alpha (M_L^2 - M_T^2) \\
 \varepsilon_{xz} &= -\varepsilon_{zx} = KM_L \\
 \varepsilon_{yz} &= -\varepsilon_{zy} = -KM_T \quad ,
 \end{aligned} \tag{6}$$

by applying a rotational transformation around the z axis to the permittivity tensor ε_{ij} (see Refs. [20, 21]). In the above equation, $\Delta G = G_{11} - G_{12} - 2G_{44}$ denotes the so-called magneto-optical anisotropy parameter.

The relation between the complex Kerr amplitude $\Phi_{s/p} = \theta_{s/p} - i\epsilon_{s/p}$ and the permittivity tensor elements ε_{ij} was thoroughly studied in literature. [2, 22] $\theta_{s/p}$ and $\epsilon_{s/p}$ denote the Kerr rotation and Kerr ellipticity for s and p polarized incident light, respectively. A general analytical expression of the Kerr effect is most often too complicated for practical uses. Therefore two important analytical approximations for ultra-thin ferromagnetic layers or bulk-like ferromagnets are often used, assuming either $t_{\text{FM}} \ll \lambda/4\pi N_{\text{FM}}$ or $t_{\text{FM}} \gg \lambda/4\pi N_{\text{FM}}$, respectively, with t_{FM} and N_{FM} being the thickness and the refractivity index of the FM layer. In both limiting cases, the analytical solution can be expressed as [23, 24, 25, 26]

$$\begin{aligned}
 \Phi_s &= -\frac{r_{ps}}{r_{ss}} = A_s \left(\varepsilon_{yx} - \frac{\varepsilon_{yz}\varepsilon_{zx}}{\varepsilon_d} \right) + B_s \varepsilon_{zx} \\
 \Phi_p &= \frac{r_{sp}}{r_{pp}} = -A_p \left(\varepsilon_{xy} - \frac{\varepsilon_{xz}\varepsilon_{zy}}{\varepsilon_d} \right) + B_p \varepsilon_{xz}
 \end{aligned} \tag{7}$$

where the weighting optical factor $A_{s/p}$ ($B_{s/p}$) is even (odd) function of the angle of incidence φ . If ε_{ij} from Eq. (4) is substituted to Eq. (7), we obtain [8]

$$\begin{aligned}
 \Phi_{s/p} &= \pm A_{s/p} \left[2G_{44} + \frac{\Delta G}{2}(1 - \cos 4\alpha) + \frac{K^2}{\varepsilon_d} \right] M_LM_T \\
 &\mp A_{s/p} \frac{\Delta G}{4} \sin 4\alpha (M_L^2 - M_T^2) \mp B_{s/p} KM_L,
 \end{aligned} \tag{8}$$

where $+$ ($-$) is related to the Kerr s (p) effect. Equation (8) is a final expression of the Kerr effect in case of an in-plane magnetized film with cubic symmetry. It shows several interesting features. (i) The last term, which is proportional to M_L , describes the ordinary LMOKE. (ii) There are two separate QMOKE contributions, being proportional to $M_L M_T$ and $M_L^2 - M_T^2$, respectively. (iii) Only the QMOKE signal strength depends on the crystallographic sample orientation α , characterized by the magneto-optic anisotropy parameter ΔG . (iv) Even if $G_{ijkl} \equiv 0$, there is a small quadratic contribution proportional to K^2 . It can be seen from Eq. (7) that this contribution originates from the mixed term $\varepsilon_{zx}\varepsilon_{yz}$ ($\varepsilon_{xz}\varepsilon_{zy}$) for Φ_s (Φ_p). This contribution is not due to an intrinsically quadratic dependence of ε_{ij} on the sample magnetization, but arises from a mixing of linear permittivity tensor components.

3. Experimental details

$\text{Co}_2\text{FeSi}(100)$ films of thicknesses 11, 21, 42 and 98 nm were prepared by RF magnetron sputtering and deposited directly onto $\text{MgO}(100)$. All film thicknesses were measured by means of X-ray reflectometry, except for the smallest thickness, which was estimated from sputtering rate and deposition time. All films grow in the L2_1 ordered structure [27, 28] and were covered by a 4 nm thick Al protective layer. A more detailed description of the sample preparation process as well as an investigation of the structural properties of such films can be found in Ref.[28]. These investigations revealed a high degree of crystalline order. In particular, no evidence for significant lattice distortions, such as those reported in Ref.[29] for the growth on $\text{GaAs}(001)$ substrates, was found during these studies.

All Kerr measurements within this article were performed using s-polarized red laser light of a wavelength of $\lambda = 670$ nm. In each case, a laser spot of $\approx 300 \mu\text{m}$ diameter was focused onto the sample surface. All hysteresis loops presented in this article were recorded when the magnetic field was applied in \mathbf{H}_8 direction (Fig. 1(b)), i.e., parallel with the plane of the incidence of the light.

4. Results and discussion

4.1. Magnetization curves

Typical Kerr rotation MOKE loops $\theta(H)$ measured on the 21 nm thick sample are presented in Fig. 2. The topmost two loops in Fig. 2 were measured at an angle of incidence of $\varphi = 45^\circ$ and a sample orientation of $\alpha = \pm 22.5^\circ$. Both loops are asymmetric as they contain LMOKE (odd in H) and QMOKE (even in H) contributions. [3, 7] The loops' asymmetric nature changes sign when the sample orientation is changed from $\alpha = 22.5^\circ$ to -22.5° , corresponding to changes of sign of the QMOKE contribution. On the other hand, when the sample orientation is 0° or 45° (not shown in Fig. 2), the loops are symmetric, which means that there is no QMOKE contribution in this

case. These results are consistent with the expected fourfold symmetry of the QMOKE contribution, see Eq. (8).

Any Kerr rotation loop can be separated into its symmetric θ_{sym} and antisymmetric θ_{asym} parts by using the relation: $\theta_{\text{sym/asym}} = [\theta_{\text{inc}}(H) \mp \theta_{\text{dec}}(-H)]/2$, where $\theta_{\text{inc/dec}}$ denotes the loop branch when H is increasing or decreasing, respectively. A more general way of the loop symmetrization and antisymmetrization valid also for systems with exchange bias has been presented by T. Mewes *et al.* [30]

The results of loop symmetrization and antisymmetrization are visualized in Fig. 2. The symmetrized (LMOKE) loops are identical for $\alpha = \pm 22.5^\circ$, so we show only one loop. Moreover, the antisymmetrized (QMOKE) loops differ only in sign in this case. Finally, the bottom loop (blue dash-dot line) shows the QMOKE loop as it is measured directly at a nearly normal angle of incidence of $\varphi \approx 0.5^\circ$ (for $\varphi = 0$, the LMOKE vanishes and hence the measured signal is proportional only to the QMOKE in the case of in-plane magnetized samples). As expected, the general shape of this QMOKE loop is identical to that of the QMOKE loops determined by antisymmetrization of the MOKE loops measured at $\varphi = 45^\circ$. However, the amplitude of the antisymmetrized QMOKE loop is slightly smaller, which can be attributed to a reduction of A_s when the angle of incidence increases [25].

4.2. Amplitude of QMOKE in saturation

In the previous section we have shown how to derive a QMOKE loop. However, it is also interesting to determine the value of the QMOKE signal in saturation. This parameter is an analogue of the LMOKE signal in saturation which is experimentally determined (in the case of Kerr rotation, for example) as $\theta_{\text{sat}, M_L} = [\theta(H_{\text{sat}}) - \theta(-H_{\text{sat}})]/2$, where H_{sat} is the saturation field of the sample. The QMOKE signal in saturation can also be determined, but in a more complicated way, [8] where the Kerr signal is subsequently measured after application of an external field in eight different directions \mathbf{H}_1 to \mathbf{H}_8 (Fig. 1(b)), which is sufficient to saturate the sample each time. In this case, [see Eq. (8)], the LMOKE Kerr rotation signal in saturation is $\theta_{\text{sat}, M_L} = [\theta(\mathbf{H}_8) - \theta(\mathbf{H}_4)]/2$, while the corresponding QMOKE signal proportional to $M_L M_T$ and $M_L^2 - M_T^2$ reads

$$\theta_{\text{sat}, M_L M_T} = [\theta(\mathbf{H}_1) + \theta(\mathbf{H}_5) - \theta(\mathbf{H}_3) - \theta(\mathbf{H}_7)]/4 \quad (9)$$

$$\theta_{\text{sat}, M_L^2 - M_T^2} = [\theta(\mathbf{H}_8) + \theta(\mathbf{H}_4) - \theta(\mathbf{H}_2) - \theta(\mathbf{H}_6)]/4. \quad (10)$$

Figure 3 displays the angular dependence of the different MOKE signals in saturation of the 21 nm thick sample at an angle of incidence of $\varphi = 0.5^\circ$. Data determined by the 8-directional method described above are represented by full symbols. In agreement with Eq. (8), it is obtained that the LMOKE signal is independent on α (■). On the other hand, the QMOKE signal related to $M_L^2 - M_T^2$ is proportional to $\sin(4\alpha)$ (▲) whereas the QMOKE signal related to $M_L M_T$ is proportional to $\cos(4\alpha) + \text{const}$ (●). The absolute vertical shift in the angular dependence of $M_L M_T$ is proportional to G_{44} [see Eq. (8)] whereas the amplitudes of both sinusoidal graphs are proportional to the anisotropy term ΔG .

The experimental data in Fig. 3 exhibit the same amplitude for both sinusoidal graphs. However, Eq. (8) shows that there is a factor of 2 between the strengths of the QMOKE contributions proportional to $M_L M_T$ and $M_L^2 - M_T^2$, respectively. This factor of 2 is effectively cancelled by the fact that $M_L M_T$ in saturation is given by $M_L M_T = M^2 \cos \alpha \sin \alpha$ and is thus equal to $1/2 M^2$ for $\alpha = 45^\circ$.

Finally it can be noted that in the case of the 21 nm thick sample (see Fig. 3), the QMOKE amplitude is 20 mdeg and the maximal QMOKE signal reaches 30 mdeg. To our knowledge, these values are the highest QMOKE amplitude and signal in reflection that have ever been measured.

4.3. Peak heights in QMOKE loops

QMOKE loops were measured in the directions of \mathbf{H}_1 to \mathbf{H}_8 for different sample orientations α . Figure 4 shows such an example of a QMOKE loop determined for the 21 nm thick sample at $\alpha = -22.5^\circ$, when the positive magnetic field was applied in \mathbf{H}_8 direction, i.e., in y -direction. The linear slope in the QMOKE loops originates from a Faraday effect arising in optical elements of the experimental setup due to the stray field of the magnet used for the measurements. The large full circle (\bullet) at $H = 0$ shows the QMOKE signal in saturation, as determined in the previous section. The value of this signal determines the absolute value of Kerr rotation in the QMOKE loop, which reaches its maxima in saturation. As the magnetic field is reduced from saturation, the QMOKE signal decreases and finally reaches zero value at the top of the peaks (i.e., at a field of H_c). Consequently, it holds that $\langle M_L M_T \rangle = 0$ and $\langle M_L^2 - M_T^2 \rangle = 0$ simultaneously during reversal, i.e., at $H = H_c$, where $\langle \dots \rangle$ indicates that these values are averaged over the laser spot area (which has a diameter of $\approx 300 \mu\text{m}$, as noted above). This fact shows that the reversal process occurs by nucleation and growth of magnetic domains. In the case of coherent magnetization reversal, the average values $\langle M_L M_T \rangle$ and $\langle M_L^2 - M_T^2 \rangle$ cannot be equal to zero simultaneously. The presence of magnetic domains during the reversal process is also confirmed by LMOKE loops measured at $\varphi = 45^\circ$, where the magnetic field was applied in transverse (x) direction and no LMOKE signal was obtained.

In order to check whether all QMOKE loops exhibited zero value at $H = H_c$, the height of the peaks was determined for loops measured at different α and at $\mathbf{H}_1 \dots \mathbf{H}_8$ directions of the applied magnetic field, as it is sketched in Fig. 4. Subsequently, these values were processed by the 8-directional method. The results obtained in this way are represented by open symbols in Fig. 3. It can be seen that for any α the QMOKE signals determined from peak heights and related to $M_L M_T$, $M_L^2 - M_T^2$ have the same value as those determined in saturation. Moreover, it can be observed that for any α the QMOKE loops are always reaching zero value during reversal at $H = H_c$. Therefore the reversal always occurs through nucleation and growth of magnetic domains, where $\langle M_L M_T \rangle = 0$ and $\langle M_L^2 - M_T^2 \rangle = 0$.

4.4. Magnetic anisotropy

Figure 5(a) shows Kerr rotation hysteresis loops determined for different film thicknesses at two different sample orientations $\alpha = \pm 22.5^\circ$. It can be observed that the hysteresis loops become more and more squared with increasing thickness while H_c is decreasing. This can most likely be attributed to an improvement of the crystalline quality of the films with increasing thickness, which leads to a higher mobility of domains walls. The reduction of H_c with increasing thickness is shown quantitatively in Fig. 5(b). For this purpose, the value of H_c was determined from symmetrized LMOKE loops, as the QMOKE contribution effectively reduces the coercivity (see Sec. 4.2). Figure. 5(b) shows that a change of film thickness from 21 nm to 98 nm results in a reduction of H_c by almost a factor of 5, i.e., from 345 Oe down to 70 Oe.

Figure 6(a) and (b) display the dependence of the coercive field H_c on the in-plane sample orientation α as determined from LMOKE symmetrized loops for all sample thicknesses. For film thicknesses of 11 nm and 21 nm, the films exhibit a very weak four-fold anisotropy, modulating H_c by less than 1%. On the other hand, a film of 98 nm thickness exhibits a weak 2-fold anisotropy, again modulating H_c by less than 1%. In the case of a Co_2FeSi film of 42 nm thickness a mixture of both a two-fold and a four-fold anisotropy seem to be present.

A similar situation is shown in Figure 6(c) and (d), which presents the dependence of relative remanence on the sample orientation α . This parameter was determined as a ratio of the LMOKE signal in zero field normalized by the value of the LMOKE signal in saturation. In this case, the modulation of the remanence is about 2% in magnitude.

The observed very weak anisotropy of H_c and remanence is very surprising, as the samples investigated here are epitaxial and therefore one should naively expect the presence of hard and easy axes. However, such hard and easy axes may still be present in our samples because, as it has been shown in Sec. 4.3, magnetization reversal occurs by domain wall propagation. Hence, the samples investigated here are unique examples of an epitaxial system, where the switching field along the hard and easy axis direction is balanced, resulting in a coercive field that is nearly independent on the sample orientation α .

4.5. Dependence of MOKE on the film thickness

Figure 7 shows the dependence of different MOKE signals on the film thickness. We present the Kerr rotation θ , the Kerr ellipticity ϵ , as well as their Pythagorean average $\Omega = \sqrt{\theta^2 + \epsilon^2}$ for both the LMOKE and QMOKE signals. Here, the QMOKE signal was determined from peak heights obtained from measurements recorded at an angle of incidence $\varphi = 45^\circ$ and a sample orientation $\alpha = 22.5^\circ$. It can be observed that the LMOKE signal (\blacktriangle) saturates at high thicknesses whereas the QMOKE signal (\triangle) reaches a maximum at an intermediate thickness and then decreases again. In order to better understand this behavior, we also measured the Kerr ellipticity in both cases, which exhibits a similar, but opposite behavior: the LMOKE Kerr ellipticity (\blacksquare)

reaches a maximum and then decreases again whereas the QMOKE Kerr ellipticity (\square) monotonically increases with increasing thickness.

Such a behavior can be attributed to the depth sensitivity of the magneto-optical Kerr effect.[2, 23, 31] This is clearly demonstrated for the Pythagorean average Ω of both the LMOKE and QMOKE signals (full and empty stars in Fig. 7). With increasing film thickness, both LMOKE and QMOKE Pythagorean averages reach their maxima at a value in the range of 20-30 nm and then saturate with further increasing thickness.

In particular, the Kerr effect amplitude originating from an ultrathin sublayer of thickness Δt situated at a depth t_i can be expressed as

$$\Phi_i \approx C \Delta t \exp \left[\frac{4i\pi t_i N_{z,\text{CFS}}}{\lambda} \right], \quad (11)$$

where $N_{z,\text{CFS}} = \sqrt{(N_{\text{CFS}}^2 - N_{\text{air}}^2 \sin^2 \varphi)}$ is the normalized (complex) k -vector in z -direction, N_{air} is the refractivity index of air and C is a complex constant.[2, 23, 31] The resulting Kerr effect amplitude Φ_{tot} is given by summation over all contributions originating from different depths, $\Phi_{\text{tot}} = \sum_i \Phi_i$. Due to the exponential term in Eq. (11), a Kerr signal originating from a deeper sublayer t_i exhibits a larger damping as well as a larger shift in phase. The Kerr signals originating from different depths t_i and t_j differ by a phase (Eq. 11) $\Delta\zeta_{i-j} = 4\pi\Re(N_{z,\text{CFS}})(t_i - t_j)/\lambda$. If the ferromagnetic films are thick and transparent enough, as in our case, then the Kerr effect amplitudes Φ_i , Φ_j from depths t_i , t_j may differ by a phase of π . In such a case, Φ_i and Φ_j cancel each other, leading to a reduction of the resulting Kerr effect amplitude, in agreement with the behavior of Pythagorean average $\Omega = |\Phi_{\text{tot}}|$ in Fig. 7.

In conclusion, the dependencies of both the Kerr rotation and ellipticity on the film thickness seem to be determined by phenomenological optical and magneto-optical properties of the investigated samples and not by a change of their electronic structures.

5. Summary and conclusions

$\text{Co}_2\text{FeSi}(100)$ films in the L2_1 structure of thicknesses 11–98 nm and deposited onto $\text{MgO}(100)$ were studied by means of the longitudinal (LMOKE) and quadratic (QMOKE) magneto-optical Kerr effect. The samples exhibit a huge QMOKE effect with an amplitude of 20 mdeg and a maximum QMOKE signal reaching 30 mdeg at a sample thickness of 21 nm. To our knowledge, these are the highest values of QMOKE amplitude and signal in reflection that have been measured so far. For example, for bcc Fe of thickness 50 nm and capped by 1.5 nm of Pd, the QMOKE signal is 5.7 mdeg.[8] Furthermore, the large QMOKE signal is a fingerprint of an exceptionally large spin-orbit coupling of second or higher order in $\text{Co}_2\text{FeSi}(100)$ compared to other FM materials [10, 32]. It should be noted that the half-metallicity also contribute significantly to large values of Kerr effect [33]. However, in our case it is also ratio QMOKE/LMOKE ≈ 0.7 signal which is much larger than in case of bcc Fe, where this ratio is about 0.1. [3]

Moreover, the investigated samples exhibit rather large coercivities of 350 or 70 Oe, corresponding to film thicknesses of 21 or 98 nm, respectively. Although they are

epitaxial, they do not show an angular dependence of the coercivity as well as the remanence in excess of 1% or 2%, respectively. More detailed investigations of the magnetization reversal process by means of Kerr microscopy might be required in order to clarify this issue. The results obtained so far strongly indicate that such reversal processes take place through nucleation and growth of magnetic domains. In particular, when the magnetic field during reversal reaches $H = H_c$, then averaging over many magnetic domains results in $\langle M_L M_T \rangle = 0$ and $\langle M_L^2 - M_T^2 \rangle = 0$ at any sample orientation α . Finally, the thickness dependence of the obtained LMOKE and QMOKE signals was found to be consistent with a phenomenological magneto-optical description. Therefore, a thickness dependence of the electronic structure of the investigated films could be excluded.

6. Acknowledgment

The project was financially supported by the Research Unit 559 "*New materials with high spin polarization*" funded by the Deutsche Forschungsgemeinschaft, and by the Stiftung Rheinland-Pfalz für Innovation. Partial support by NEDO International Joint Research Program 2004IT093 of the Japanese government, by European Commission within the EU-RTN ULTRASWITCH (HPRN-CT-2002-00318) and by Grant Agency of the Czech Republic (202/06/0531) is gratefully acknowledged. We would like to thank T. Mewes for stimulating discussions.

7. References

- [1] Kerr J 1877 *Philos. Mag.* **3** 321
- [2] Hubert A, Schäfer R. Magnetic Domains: The Analysis of Magnetic Microstructures. Berlin: Springer-Verlag; 1998
- [3] Postava K, Jaffres H, Schuhl A, Nguyen Van Dau F, Goiran M, Fert AR 1997 *J. Magn. Magn. Mater.* **172** 199
- [4] Cowburn RP, Ferré J, Jamet JP, Gray SJ, Bland JAC 1997 *Phys. Rev. B* **55** 11593
- [5] Mattheis R, Quednau G 1999 *J. Magn. Magn. Mater.* **205** 143
- [6] Moore GP, Ferré J, Mougin A, Moreno M, Däweritz L 2003 *J. Appl. Phys.* **94** 4530
- [7] Osgood III RM, Bader SD, Clemens BM, White RL, Matsuyama H 1998 *J. Magn. Magn. Mater.* **182** 297
- [8] Postava K, Hrabovský D, Pištora J, Fert AR, Višňovský Š, Yamaguchi T 2002 *J. Appl. Phys.* **91** 7293
- [9] Hulme HR 1932 *Proc. R. Soc. London* **A135** 237
- [10] Bruno P, Suzuki Y, Chappert C 1996 *Phys. Rev. B* **53** 9214
- [11] Wurmehl S, Fecher GH, Kandpal HC, Ksenofontov V, Felser C, Lin HJ 2006 *Appl. Phys. Lett.* **88** 032503
- [12] Inomata K, Okamura S, Miyazaki A, Kikuchi M, Tezuka N, Wojcik M, Jedryka E 2006 *J. Phys. D: Appl. Phys.* **39** 816
- [13] Kallmayer M, Elmers HJ, Balke B, Wurmehl S, Emmerling F, Fecher GH, Felser C 2006 *J. Phys. D: Appl. Phys.* **39** 786
- [14] Kandpal HC, Fecher GH, Felser C, Schönhense G 2006 *Phys. Rev. B* **73** 094422
- [15] Hashimoto M, Herfort J, Schönherr HP, Ploog KH 2006 *Appl. Phys. Lett.* **87** 102506
- [16] Wurmehl S, Fecher GH, Kandpal HC, Ksenofontov V, Felser C, Lin HJ, Morais J 2005 *Phys. Rev. B* **72** 184434
- [17] Tezuka N, Okamura S, Miyazaki A, Kikuchi M, Inomata K 2006 *J. Appl. Phys.* **99** 08T314
- [18] Niculescu V, Budnick JI, Hines WA, Raj K, Pickart S, Skalski S 1979 *Phys. Rev. B* **19** 452
- [19] Višňovský Š 1986 *Czech. J. Phys. B* **36** 625
- [20] Postava K, Pištora J, Yamaguchi T, Hlubina P. Polarized light in structures with magnetic ordering. In: Pluta M, Szyjer M, Powichrowska E, editors. Lightmetry 2002: Metrology and Testing Techniques Using Light vol. 5064 of Proc. of SPIE Bellingham, Wash.: SPIE; 2003. p. 182–190
- [21] Višňovský Š 1986 *Czech. J. Phys. B* **36** 1424
- [22] Zvezdin AK, Kotov VA. Modern Magnetooptics and Magneto-optical Materials. London: Taylor & Francis; 1997
- [23] Traeger G, Wenzel L, Hubert A 1992 *Phys. Stat. Sol. (a)* **131** 201
- [24] Qiu Z, Bader S 1999 *J. Magn. Magn. Mater.* **200** 664
- [25] Višňovský Š, Nývlt M, Prosser V, Lopusník R, Urban R, Ferré J, Pénissard G, Renard D, Krishnan R 1995 *Phys. Rev. B* **52**(2) 1090
- [26] Hamrle J, Ferré J, Jamet JP, Repain V, Baudot G, Rousset S 2003 *Phys. Rev. B* **67**(15) 155411
- [27] Wurmehl S, Fecher GH, Kroth K, Kronast F, Dürr HA, Takeda Y, Saitoh Y, Kobayashi K, Lin HJ, Schönhense G, Felser C 2006 *J. Phys. D: Appl. Phys.* **39** 803
- [28] Schneider H, Jakob G, Kallmayer M, Elmers HJ, Cinchetti M, Balke B, Wurmehl S, Felser C, Aeschlimann M, Adrian H 2006 *Phys. Rev. B* **74** 174426
- [29] Hashimoto M, Herfort J, Schönherr HP, Ploog KH 2006 *J. Phys. Condens. Matter* **18** 6101
- [30] Mewes T, Nembach H, Rickart M, Hillebrands B 2004 *J. Appl. Phys.* **95** 5324
- [31] Hamrle J, Ferré J, Nývlt M, Višňovský Š 2002 *Phys. Rev. B* **66**(22) 224423
- [32] Hamrle J, Blomeier S, Gaier O, Hillebrands B, Schneider H, Jakob G, Reuscher B, Brodyanski A, Kopnarski M, Postava K, Felser C 2007 *J. Phys. D: Appl. Phys.* (in press); cond-mat/0609633
- [33] van Ek J, Huang W, MacLaren JM 1997 *J. Appl. Phys.* **81** 5429

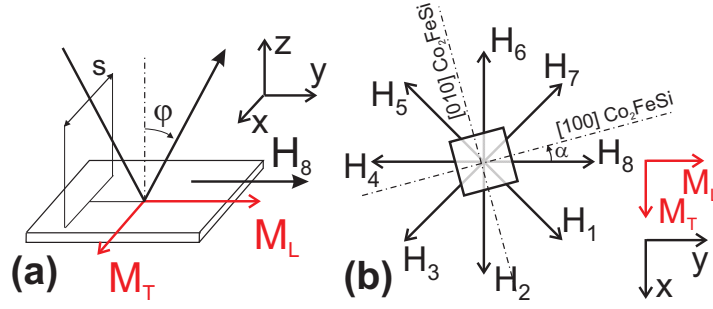


Figure 1. (color online) (a) Sketch of the sample and the incident s-polarized light. (b) Definition of the 8 directions of the externally applied magnetic field which are used to determine the values of the QMOKE signal in saturation. α denotes the sample orientation, i.e., the angle between the $[100] \text{Co}_2\text{FeSi}(100)$ direction and the plane of incidence of the incoming light (y -axis). All hysteresis loops presented in this article were recorded when the positive direction of the magnetic field corresponds to \mathbf{H}_8 direction, i.e., parallel with the plane of the incidence of the light.

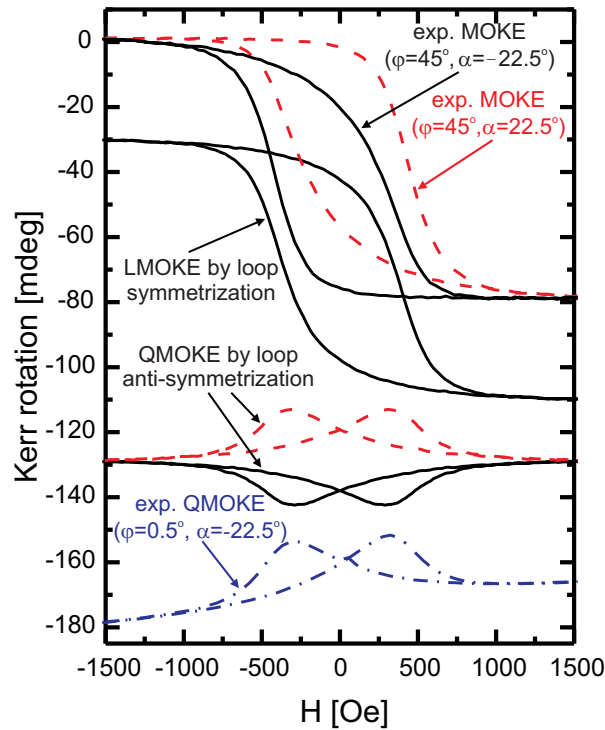


Figure 2. (color online) MOKE loops recorded from the $\text{Co}_2\text{FeSi}(100)(21 \text{ nm})$ sample. The topmost two loops were directly measured at $\varphi = 45^\circ$ and $\alpha = 22.5^\circ$ (red dashed line) or $\alpha = -22.5^\circ$ (black full line), respectively. These two loops are symmetrized and anti-symmetrized (see text for details), providing LMOKE and QMOKE contributions. The bottom loop (blue dash-dotted line) is a QMOKE loop directly measured at $\varphi = 0.5^\circ$ and $\alpha = -22.5^\circ$.

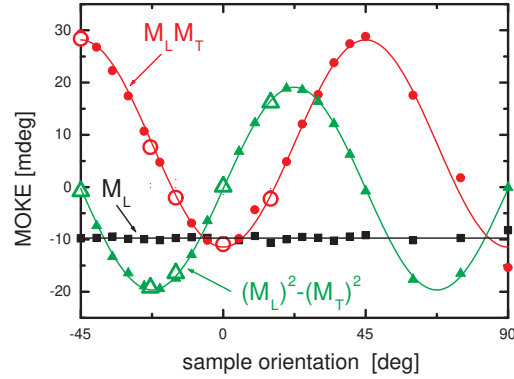


Figure 3. (color online) (full symbols) Dependence of different MOKE signals in saturation for the $\text{Co}_2\text{FeSi}(100)(21\text{ nm})$ sample on the sample orientation α at $\varphi = 0.5^\circ$, which are determined from the 8-directional method [8]. (open symbols) MOKE signals determined from the height of peaks in QMOKE loops. See text for details.

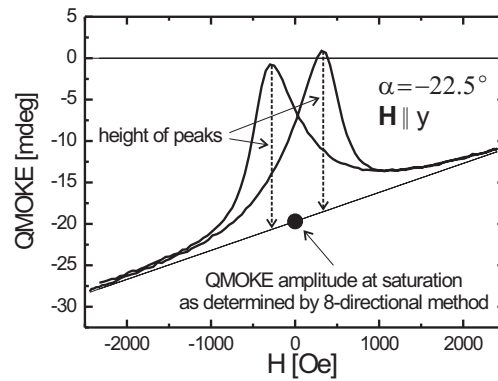


Figure 4. QMOKE Kerr rotation loop in $\text{Co}_2\text{FeSi}(100)(21\text{ nm})$ measured at $\varphi = 0.5^\circ$, at a sample orientation $\alpha = -22.5^\circ$, and within positive field ranges applied in $\mathbf{H}_8 \parallel y$ direction. The full circle at $H = 0$ shows the QMOKE signal in saturation as determined by the 8-directional method for this particular α . Dashed arrows illustrate how the height of the peaks in the QMOKE loop is determined. It can be seen that the QMOKE reaches its maximum when the sample is in saturation. Furthermore, the QMOKE is zero when the peaks are reaching their highest signal.

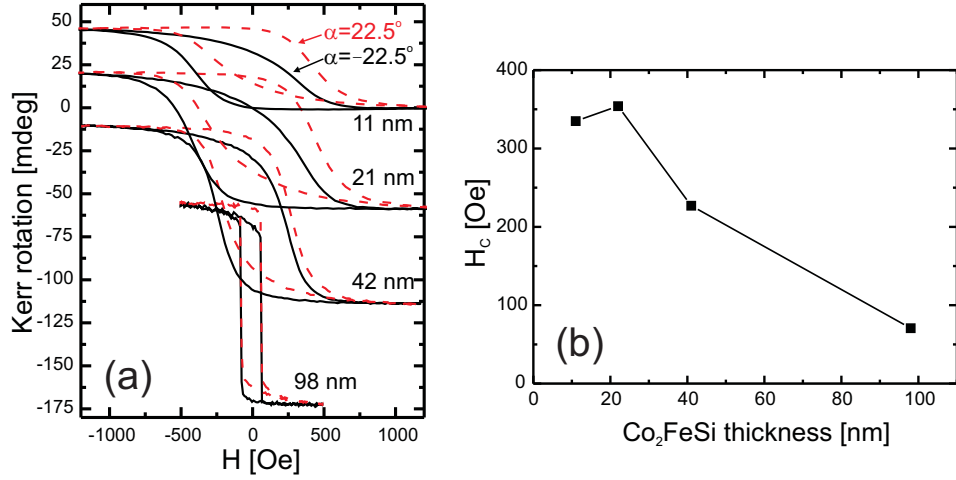


Figure 5. (color online) (a) MOKE hysteresis loops for different thicknesses of $\text{Co}_2\text{FeSi}(100)$ films, recorded at an angle of incidence $\varphi = 45^\circ$. The sample orientation is equal to 22.5° (dashed red line) or -22.5° (full black line). (b) Dependence of H_c on Co_2FeSi film thickness.

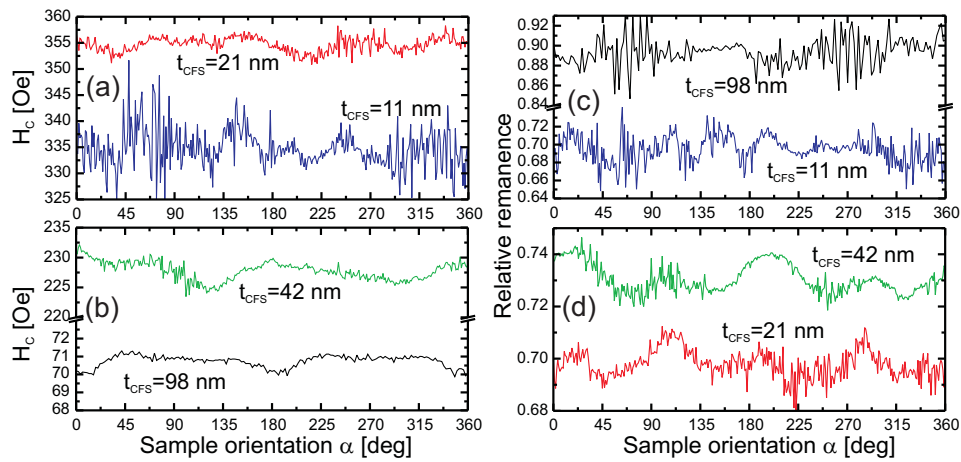


Figure 6. (color on-line) Dependence of (a)(b) the coercive field and (c)(d) the relative remanence on the sample orientation α as determined from symmetrized LMOKE loops in Co_2FeSi films. The relative remanence is determined as the ratio of the LMOKE signal at $H = 0$ Oe and the LMOKE signal in saturation.

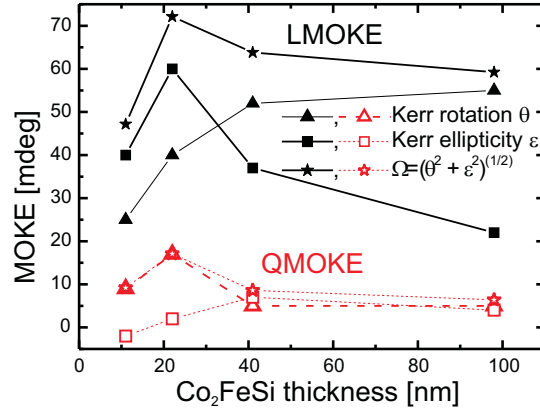


Figure 7. (color online) Dependence of the LMOKE and QMOKE signals at saturation on the film thickness, measured at $\varphi = 45^\circ$. The QMOKE signal was determined from the height of peaks in QMOKE loops, which are obtained by antisymmetrization of experimental MOKE loops.